Journal of
CHEMOMETRICS WILEY

Semi-quantification of binary saline solutions by Raman spectroscopy: Implications for Europa

Jose Antonio Manrique[1,2] | **Marco Veneranda**[1] | **Yaiza Merino-Lomas**[1] | **Fernando Rull**[1] | **Elena Charro**[1] | **Manuel A. Gonzalez**[1] | **Jose Manuel Lopez**[1] | **Eduardo Rodríguez Gutiez**[1] | **Jose Aurelio Sanz-Arranz**[1] | **Sylvestre Maurice**[2] | **Guillermo Lopez-Reyes**[1]

[1]University of Valladolid, Valladolid, Spain

[2]Institut de Recherche en Astrophysique et Planétologie, Université de Toulouse 3 Paul Sabatier, CNRS, CNES, Toulouse, France

Correspondence

Jose Antonio Manrique, University of Valladolid, Paseo de Belén, 7, 47011 Valladolid, Spain.
Email: joseantonio.manrique@uva.es

Abstract

The Europa lander is a concept for a potential future planetary exploration mission which purpose is to characterize the icy shell of Europa and to search for organics. To achieve this objective, the current concept of the lander includes a Raman spectrometer, such as RLS instrument, that could be able to analyze (sub) surface targets in their solid and liquid form. Knowing that ice and brines of Europa are potentially enriched by sulfate and chlorides, this work seeks to evaluate if Raman spectroscopy could be used to semi quantify the saline content of water solutions using space-like instrumentation. To do so, $MgSO_4$ and $MgCl_2$ were used to prepare three sets of water solutions. Raman analyses were then performed by the laboratory simulator of the ExoMars Raman Laser Spectrometer (RLS), which has been defined as the threshold system for the Europa Lander. After data analysis, two different semi-quantification approaches were tested, and their results compared. Although univariate calibration curves proved to successfully quantify the content of SO_4^{2-} and Cl^- anions dissolved in mono-analyte water solutions, this strategy provided very poor results when applied to binary saline mixtures. Overcoming this issue, the non-linearity prediction ability of Artificial Neural Networks (ANNs) in combination with bandfitting allows to successfully resolve the complexity of the vibrational perturbation suffered by the OH region, which is caused by the cross interaction of H_2O molecules with different anions.

KEYWORDS

artificial neural networks, Europa, Raman, saline solution, semi-quantification

1 | INTRODUCTION

Current efforts in investigating the potential presence of life outside terrestrial domains mainly focus on the robotic exploration of Mars. Successfully landed at Jezero Crater on February 2021, the Perseverance rover (NASA/Mars 2020 mission[1]) is using complementary spectroscopic techniques (SuperCam,[2–4] Sherloc[5] and PIXL[6]) to detect astrobiology relevant targets. The selected materials will be fetched and stored in hermetic tubes that will be eventually returned to Earth through a dedicated Mars Sample Return Campaign.[7] In addition to that, the ExoMars missions lead by ESA will soon deploy the Rosalind Franklin rover at Oxia Planum.[8] Here, the molecular investigation performed by Raman Laser Spectrometer (RLS[9]) and MicrOmega[10] instruments will be crucial in the selection of putative biomarkers-bearing samples to be analyzed by the Mars Organic Molecule Analyser.[11] Both missions are considered a milestone in the application of Raman spectroscopy in Space exploration, being ExoMars, the first mission that included a Raman instrument in its payload, and Mars2020 the first to actually deploy and use Raman instruments in a planetary body other than Earth.

Looking ahead, Europa has been pointed out as the primary target to extend the search for life toward the Outer Solar System. Although covered by an outer icy shell, it is widely believed the underlying ocean is providing a long-term, stable environment in which a second, independent origin of life might have arisen.[12,13] Knowing that the dynamics in Europa's crust allow the underlying ocean not to be isolated from the surface[14] but to exchange material with the outer crust, it is believed that potential organics and biomarkers could be present at the surface of its icy shell.

Taking into account its outstanding astrobiological potential, the exploration of Europa was remarked in the last two Planetary Decadal Surveys (2003[15] and 2013[16]). On one hand, the proposed orbiter (Europa Clipper) is currently under development and is expected to be launched in 2024.[17] On the other hand, the Europa Lander mission is still in phase of definition. As described elsewhere, the high-level science goals of the Europa Lander Mission Concept (ELMC) are (1) to search for traces of life; (2) to evaluate the habitability of Europa via in-situ techniques; and (3) to investigate surface and subsurface properties to support future exploration.[18] To achieve these goals, the NASA Science Definition Team (SDT) proposed a payload composed of a seismometer, a context imager, an optical microscope, desirably with spatially resolved spectroscopic capabilities, a mass spectrometer, and a Raman spectrometer.[18]

Being capable of detecting both inorganic and organic compounds, the Raman spectrometer will be crucial in addressing the three main science objectives of the mission. In this regards, the STD report identifies a SHERLOC-like instrument as the baseline, and a RLS-like instrument as the threshold to be selected as the Raman system for the Europa Lander.[18] Paving the way to the development of a dedicated Raman spectrometer for the mission, interesting analytical solutions have been recently proposed.[19,20] Among them, the Compact Integrated Raman Spectrometer (CIRS[21]) has been granted through the Instrument Concepts for Europa Exploration (ICEE-2) program, which offers a preliminary definition of a payload for the lander.[22] As defined in a dedicated work, the Sample Handling System (SHS) coupled to CIRS enables the analysis of samples in their frozen, melted, and desiccated states, thus enhancing the characterization of, non-volatile constituents as well as ions and putative organic molecules potentially dissolved in the water.[21]

Although the CIRS team is advancing the technical readiness of the Raman instrument for the ELMC, literature shows an increasing number of research works aimed at defining the potential scientific outcome of Raman spectroscopy at Europa. To achieve this purpose, the analysis of terrestrial analogue sites[23–25] is complemented by the laboratory investigation of simulant samples reproducing the composition of Europa's ice and brines.[26–29]

As such, previous investigations suggest the ocean and the icy shell of Europa contain high concentrations of Mg and Ca sulfates (up to 30%),[30] together with minor amounts of chlorides,[31] among others. Knowing the salt content and composition of H_2O samples can play an important role either in limiting (e.g., by negatively affecting the osmotic balance[32]) or promoting the proliferation of life (e.g., by providing the chemical energy needed for metabolic reactions[33,34]) the proliferation of life, the capability of Raman spectroscopy to investigate crystalline salts and their dissolved ions makes it the key tool to assess the astrobiology potential of Europa samples.

In this regards, Raman spectroscopy can be effectively used to determine the molarity of water solutions containing Raman-active polyatomic ions such as sulfate, nitrate and carbonate.[35,36] In addition to that, the semi-quantification of Raman-inactive monoatomic ions (e.g., chloride) can also be inferred by investigating their effect on the vibration dynamics of the water.[37,38]

When analyzing mono-analyte solutions, the semi-quantification of both polyatomic- and monoatomic-anions can be successfully achieved using external calibration curves.[35,39] On the contrary, the investigation of complex solutions presenting a mixture of both monoatomic and polyatomic ions (as is the expected case for Europa) introduces a higher

degree of complexity that can only be addressed through more elaborated chemometric tools. Despite being of crucial importance to optimize the scientific outcome of Raman spectra, there is a lack of studies evaluating the use of Artificial Neural Networks analysis (ANNs[40]) to interpret Raman spectra from Europa-representative binary solutions. Filling the lack of literature, this work investigates the potential use of ANNs as a tool to semi quantify the content of both Raman active (sulfate) and inactive (chloride) ions contained in complex saline solutions according to their Raman spectrum.

2 | MATERIALS AND METHODS

2.1 | Sample preparation

Three different sets of saline solutions were prepared by mixing pure salts (ACS reagent grade, >99.0%) with de-ionized water. Considering the expected salt content of Europa ice and brines (see section 1), magnesium sulfate ($MgSO_4$) and magnesium chloride ($MgCl_2$) were used to enrich the solutions with representative polyatomic (SO_4^{2-}, Raman-active) and monoatomic (Cl^+, Raman-inactive) ions, respectively. As represented in Table 1, two sets of mono-analyte solutions were prepared. Afterwards, a third set of binary solutions was prepared by mixing both salts at different concentration ratios. Each solution was introduced in a 4.5 ml glass vial, and Raman analysis were performed directly on liquid. This analytical procedure is considered to be representative of the future Europa Lander mission, as the design concept of the CRISM Raman spectrometer includes a sample handling system that allows ice samples to be analyzed in their frozen form.

2.2 | Raman analysis

Raman spectra of the prepared solutions were acquired using the laboratory simulator of the ExoMars RLS, which was selected by the STD as the threshold of the Raman system to be deployed on Europa.[18] As detailed elsewhere[41] the instrument has been assembled at the University of Valladolid by using commercial components, including a green laser source, a high resolution TE Cooled CCD Array spectrometer and an optical head with a long WD objective of 50×. Excitation wavelength (532 nm), range of analysis (100–4200 cm^{-1}), spot of analysis (≈50 μm) and spectral resolution (6–10 cm^{-1}) of this instrument are closely resembling the requirement established by the STD for the Raman onboard the future Europa Lander. Twenty spectra per sample were autonomously acquired using a custom developed software based on LabVIEW 2013 (National Instruments). To do so, the RLS-Sim integrates the same algorithms implemented by the RLS flight model, such as dark subtraction, fluorescence quenching and acquisition parameters calculation.[42]

TABLE 1 List of $MgSO_4$, $MgCl_2$, and $MgSO_4$–$MgCl_2$ aqueous solutions prepared for this work

(a) MgSO₄ solutions set		(b) MgCl₂ solutions set		(c) Binary solutions set	
MgSO₄ (g/100 ml)	MgCl₂ (g/100 ml)	MgSO₄ (g/100 ml)	MgCl₂ (g/100 ml)	MgSO₄ (g/100 ml)	MgCl₂ (g/100 ml)
5	0	0	5	5	10
15	0	0	10	5	60
20	0	0	15	10	30
25	0	0	20	10	60
30	0	0	30	30	10
40	0	0	40	30	30
50	0	0	50	60	10
60	0	0	60	60	30
70	0	0	70	60	60
100	0	0	100		

2.3 | Data treatment and interpretation

Before processing the data with chemometric methods, Raman spectra were submitted to normalization and baseline correction using the SpectPro software.[43,44] Afterwards, a dedicated MATLAB routine was created to run a data pretreatment based on band fitting. As presented in previous works, the OH region of the water (from 3000 to 3700 cm^{-1}) was fitted with five Gaussian-Lorentzian sub-bands (this being the ideal line shape fitting spectral peaks), whose wavelength positions were fixed at 3014, 3224, 3430, 3572, and 3636 cm^{-1}, respectively. Similarly, the characteristic main peak of the sulfate ion was fitted using one Gaussian-Lorentzian sub-band located at 981 cm^{-1}. After automatic band-fitting, the characteristic parameters of the employed sub-bands (intensity, area, Gauss/Lorentz ratio and full width at half maximum value) were extrapolated. The data matrix was finally employed for chemometric analysis. On one hand, standard univariate calibration curves were created and used to predict the concentration of the investigated analytes. On the other hand, the whole data matrix was used as the input layer for the ANN model (created in MATLAB environment). In this last step, the band fitting itself was used as a pre-processing for multivariate analyses, obtaining a dimensionality reduction, and coping with the noise from the spectra at this stage. This said, our system is them described in terms of 16 variables: one variable corresponding to the intensity of the sulfate band, and three variables to describe each of the individual bands of the band fitting of the OH region, we left the position of each band out, as they remained constant by experimental design.

3 | RESULTS

The characteristic peaks of a Raman-active salt in a solution usually increase in intensity with the concentration. As such, a reliable Raman-based semi-quantification of the analyte is generally achieved by building external calibration curves in which the characteristic spectral indicator of the anion is plotted as a function of the concentration. In the case of saline solutions containing Raman-active polyatomic anions such as sulfate, nitrate, and carbonate, the intensity or the area of their main Raman peak (corresponding to the symmetric stretching vibration centered at 981, 1047, and 1066 cm^{-1}, respectively) is generally selected as the spectral indicator of the analyte.[36,45] To achieve a reliable correlation of the data, the selected indicator needs to be measured after the normalization of the spectra.[36] Although several normalization procedures have been proposed, most works related to the analysis of aqueous solutions consider the normalization of the Raman spectra to the area or intensity of the OH stretching region of the water, which is comprised within the range that goes from 3000 to 3700 cm^{-1}.[46] Having in mind that ice and brines at Europa are believed to be enriched of sulfates, literature presents several works in which the mentioned method has been successfully used to semi-quantify the saline content of aqueous SO_4^{2-} solutions.[35,46]

Knowing that most of the referenced works are based on the use of state-of-the-art Raman instruments, a calibration curve was built to evaluate to which degree the reliability of the univariate quantification procedure is affected by the lower resolution of spectrometers designed to be used in space exploration missions. As such, the RLS-Sim was used to automatically collect 20 spectra from each of the sulfate solutions described in Table 1a. After baseline correction, all spectra were normalized to the area of the OH region. After averaging the 20 spectra per sample, the intensity of the characteristic peak of sulfate at 981 cm^{-1} was finally plotted as a function of its concentration. As represented in Figure 1, the obtained calibration curve provides a correlation coefficient R^2 equal to 0.9978 which is in line with the results obtained by high-resolution spectrometers. In this sense, it must be also highlighted that calibration curves obtained by averaging a smaller number of spectra returned lower correlation coefficient (0.9786, 0.9629, and 0.9435 when averaging 15, 10, and 5 spectra respectively), thus proving how the higher the number of accumulations, the better the performance of the instrument, which is capital in flight instruments that, usually, are not as powerful as benchtop instrumentation.

The equation describing the calibration curve (X = 129558y^2 + 1621.6y + 2.3867) was used to semi-quantify the sulfate content of the binary solutions listed in Table 1c. As shown in Figure 1 the plotted results (red markers) demonstrate that, despite being a non-Raman active salt, the presence of $MgCl_2$ strongly affects the semi-quantitative determination of sulfate, leading to its underestimation. As representative example, the intensity of the main $SO4^{2-}$ peak (after normalization) of the samples prepared with 60 mg of sulfate, decrease from 0.016195 (mono-analyte solution) to 0.01498345 (−7.49%), 0.01102598 (−31.92%), and 0.00210204 (−87.02%) when adding 10, 30, and 60 mg of $MgCl_2$, respectively. The same trend was observed in all binary solutions, which indicates the underestimation of the sulfate content is directly proportional to the content of the second salt the solution. This is due to the change in
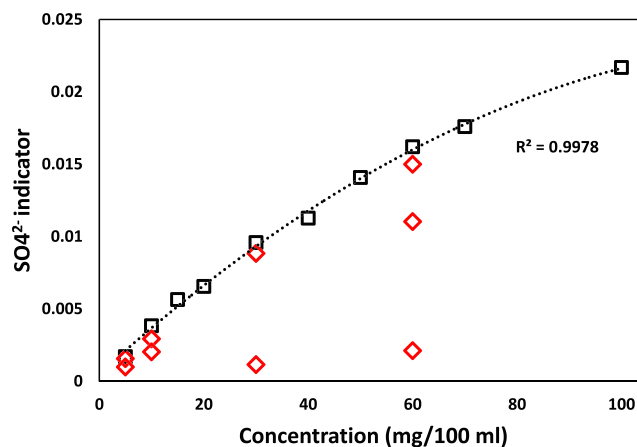
FIGURE 1   calibration curve to semi-quantify the SO_4^{2-} content in water solutions. Black markers represent the 20 spectra-averaged values of mono-analyte $MgSO_4$ solutions, whereas red markers represent binary $MgSO_4$–$MgCl_2$ solutions.

proportionality between the sulfate band intensity and the total area of OH region as a consequence of the change in the vibrational dynamics of the water molecules.

By investigating this phenomenon, Qiu et al.[46] proved the intensity of the sulfate peak at 981 cm^{-1} is not affected by the presence of chloride in the solution. On the contrary, the vibrational profile of the water is strongly affected by the salinity of the solution. In this sense, it is well known that H_2O molecules tend to form hydrogen bonding interactions with the neighboring molecules, where OH acts as proton donor (D) and/or proton acceptor (A).[47] On one hand, the electronic perturbation triggered by positively charged ions (in this study, Mg^{2+}) interacting with the hydrogen (acceptor) is so small that their effect on the vibrational profile can be barely detected by conventional Raman spectrometers.[38,48,49] On the other hand, negatively charged ions (in this study SO_4^{2-} and Cl^-) strongly interact with the hydrogen (donor) side of water molecules, thus triggering clear changes of their OH profile.[38,49] The detailed analysis of Raman bands of liquid water suggests the OH stretching band is the result of the contribution of five different sub-vibrations that can be classified as DAA (single donor–double acceptor, peak at 3014 cm^{-1}), DDAA (double donor–double acceptor, Raman peak centered at 3226 cm^{-1}), DA (single donor–single acceptor 3432 cm^{-1}), DDA (double donor–single acceptor, peak at 3572 cm^{-1}), and free OH (3636 cm^{-1}).[47] Knowing this, previous studies experimentally proved the dissolved anions affect the OH vibrations mainly by weakening the DDAA mode (centered at 3226 cm^{-1}) and reinforcing the DA mode (centered at 3432 cm^{-1}).

In order to define the contribution of DDAA, DDA, DAA, DA, and free OH vibrational modes on the salinity-related evolution of the OH region, the band fitting of the normalized area was carried out by a dedicated MATLAB routine that kept the position of five Gaussian/Lorentzian bands (this being the curve better suited to describe Raman peaks[50]) fixed at 3014, 3226, 3432, 3572, and 3636 cm^{-1} (allowing a shift of ± 4 cm^{-1}) while adjusting their intensity, width and Gaussian/Lorentzian ratio. With regards to the sulfate bearing solutions, an additional band fitting was carried out to extrapolate the intensity value of the characteristic peak of SO_4^{2-} ions centered at 981 cm^{-1}. After averaging the results obtained from each of the 20 spectra collected from each solution, the values of the 16 spectral parameters are provided in Table 2.

Focusing on the study of the OH region, Figure 2 displays the results of the automated band fitting performed on the solutions containing different concentration of $MgCl_2$. By increasing the salinity from 10 to 100 mg/100 ml, band deconvolution results in a clear weakening of the DDAA vibrational mode (also known as strong hydrogen bonding component HBS) and a simultaneous reinforcement of the DA one (also known as weak hydrogen bonding component HBW).

Although the increase in salinity causes marked changes in the intensities of DDAA and DA vibrational modes, when the spectra are area normalized in the OH region, an isosbestic point is clearly visible.[46] This proves that, when the dynamics of water change due to salinity, the oscillator population change from one configuration to other, but the global number of oscillators is kept constant.[38] Knowing the magnitude of DDAA intensity decrement is similar to the DA increment, the sum of the two peak intensities have been previously used as internal reference to build Raman semi-quantification models of chloride solutions.[38,46] Similarly, in this work the ratio $I_{DDAA}/(I_{DDAA} + I_{DA})$ has been used as spectral indicator to build the Cl^- calibration curve presented in Figure 3.

TABLE 2 Spectral parameters extrapolated through the automated band fitting of the Raman spectra

Set	Sample MgSO$_4$ (mg/100 ml)	MgCl$_2$ (mg/100 ml)	SO$_4^{2-}$ (981 cm^{-1}) Intensity	DAA-OH (3014 cm^{-1}) Intensity	G/L ratio	Width	DDAA-OH (3226 cm^{-1}) Intensity	G/L ratio	Width
MgSO$_4$–H$_2$O	0	0	1.80E-05	4.52E-05	9.58E-01	2.05E+01	1.77E-03	8.01E-01	2.12E+02
	5	0	1.69E-03	1.54E-05	9.79E-01	2.01E+01	1.34E-03	8.38E-01	1.65E+02
	10	0	3.83E-03	4.15E-05	9.78E-01	2.07E+01	1.28E-03	7.54E-01	1.63E+02
	15	0	5.64E-03	2.01E-04	9.76E-01	2.27E+01	1.60E-03	7.33E-01	1.50E+02
	20	0	6.55E-03	3.87E-05	9.58E-01	2.07E+01	1.21E-03	7.22E-01	1.62E+02
	30	0	9.58E-03	2.51E-05	9.79E-01	2.03E+01	1.23E-03	8.26E-01	1.57E+02
	40	0	1.13E-02	3.03E-05	9.80E-01	2.03E+01	1.27E-03	9.07E-01	1.68E+02
	50	0	1.41E-02	7.14E-05	5.20E-01	2.13E+01	1.07E-03	4.76E-01	1.45E+02
	60	0	1.62E-02	3.26E-05	9.79E-01	2.04E+01	1.11E-03	7.75E-01	1.53E+02
	70	0	1.76E-02	3.98E-05	9.79E-01	2.06E+01	1.07E-03	7.89E-01	1.52E+02
	100	0	2.17E-02	3.80E-05	9.80E-01	2.06E+01	1.02E-03	8.00E-01	1.52E+02
MgCl$_2$–H$_2$O	0	0	1.80E-05	4.52E-05	9.58E-01	2.05E+01	1.77E-03	8.01E-01	2.12E+02
	0	5	1.21E-04	2.61E-05	9.79E-01	2.03E+01	1.41E-03	9.17E-01	1.64E+02
	0	15	4.50E-05	2.87E-05	9.80E-01	2.03E+01	1.21E-03	8.11E-01	1.55E+02
	0	20	2.28E-04	6.57E-05	8.66E-01	2.10E+01	9.69E-04	5.71E-01	1.30E+02
	0	25	2.98E-05	2.32E-05	9.80E-01	2.03E+01	1.06E-03	8.78E-01	1.46E+02
	0	30	3.45E-05	2.54E-05	9.80E-01	2.03E+01	8.98E-04	8.14E-01	1.38E+02
	0	40	4.86E-05	3.90E-05	9.80E-01	2.06E+01	7.63E-04	7.06E-01	1.15E+02
	0	50	2.36E-04	7.34E-05	3.08E-01	2.21E+01	5.93E-04	5.61E-01	1.09E+02
	0	60	4.39E-05	3.83E-05	8.49E-01	2.07E+01	6.21E-04	7.13E-01	1.09E+02
	0	70	1.95E-04	6.75E-05	1.31E-01	2.16E+01	5.07E-04	4.66E-01	1.03E+02
	0	100	1.64E-04	4.21E-05	1.34E-01	3.02E+01	4.34E-04	1.68E-01	1.06E+02
MgSO$_4$–MgCl$_2$–H$_2$O	5	10	1.56E-03	2.91E-05	9.80E-01	2.03E+01	1.12E-03	7.02E-01	1.51E+02
	5	60	9.74E-04	5.03E-05	6.87E-01	2.09E+01	6.82E-04	5.71E-01	1.22E+02
	10	30	2.92E-03	4.26E-05	9.80E-01	2.07E+01	7.10E-04	7.04E-01	1.14E+02
	10	60	2.03E-03	4.47E-05	2.51E-01	2.29E+01	4.93E-04	7.93E-01	1.03E+02
	30	10	8.83E-03	5.97E-05	4.74E-01	2.13E+01	9.05E-04	6.59E-01	1.34E+02
	30	30	1.14E-03	3.41E-05	9.80E-01	2.04E+01	1.26E-03	8.15E-01	1.50E+02
	60	10	1.50E-02	6.53E-05	7.89E-01	2.21E+01	8.19E-04	5.96E-01	1.31E+02
	60	30	1.10E-02	3.77E-05	9.80E-01	2.08E+01	8.24E-04	8.12E-01	1.40E+02
	60	60	2.10E-03	2.26E-05	9.80E-01	2.02E+01	1.15E-03	7.27E-01	1.43E+02

TABLE 2 (Continued)

Set	DA-OH (3433 cm⁻¹)			DDA-OH (3572 cm⁻¹)			Free OH (3536 cm⁻¹)		
	Intensity	G/L ratio	Width	Intensity	G/L ratio	Width	Intensity	G/L ratio	Width
MgSO$_4$–H$_2$O	2.18E-03	9.42E-01	2.20E+02	3.48E-04	8.94E-01	1.19E+02	2.57E-04	3.22E-01	7.38E+01
	2.78E-03	9.77E-01	2.43E+02	1.96E-04	9.15E-01	6.27E+01	3.22E-04	9.40E-01	6.06E+01
	2.75E-03	9.15E-01	2.45E+02	1.47E-04	3.56E-01	4.27E+01	2.60E-04	9.79E-01	6.12E+01
	3.00E-03	7.72E-01	2.14E+02	4.01E-04	6.81E-01	4.38E+01	4.41E-04	9.71E-01	5.31E+01
	2.78E-03	9.39E-01	2.48E+02	1.28E-04	6.22E-01	4.10E+01	2.13E-04	9.43E-01	5.95E+01
	2.96E-03	9.77E-01	2.42E+02	9.25E-05	6.44E-01	3.70E+01	2.09E-04	8.78E-01	5.48E+01
	2.90E-03	9.74E-01	2.46E+02	9.42E-05	7.52E-01	2.59E+01	1.50E-04	9.79E-01	5.22E+01
	2.91E-03	8.90E-01	2.46E+02	6.27E-05	9.50E-01	2.65E+01	1.55E-04	9.30E-01	3.00E+01
	3.08E-03	9.75E-01	2.44E+02	6.33E-05	9.60E-01	2.66E+01	1.17E-04	9.60E-01	3.98E+01
	3.10E-03	9.67E-01	2.44E+02	5.61E-05	9.61E-01	2.38E+01	1.05E-04	9.80E-01	3.44E+01
	3.17E-03	9.71E-01	2.43E+02	4.56E-05	9.52E-01	2.29E+01	8.51E-05	9.80E-01	2.29E+01
MgCl$_2$–H$_2$O	2.18E-03	9.42E-01	2.20E+02	3.48E-04	8.94E-01	1.19E+02	2.57E-04	3.22E-01	7.38E+01
	2.82E-03	9.27E-01	2.40E+02	1.47E-04	4.10E-01	5.37E+01	2.45E-04	9.13E-01	5.22E+01
	3.02E-03	9.43E-01	2.41E+02	1.28E-04	6.74E-01	5.26E+01	2.12E-04	9.56E-01	4.66E+01
	3.19E-03	8.40E-01	2.33E+02	1.32E-04	8.72E-01	6.30E+01	2.01E-04	7.79E-01	4.10E+01
	3.20E-03	9.75E-01	2.40E+02	8.42E-05	8.95E-01	5.58E+01	1.54E-04	9.67E-01	4.90E+01
	3.29E-03	9.70E-01	2.40E+02	1.51E-04	9.29E-01	5.95E+01	1.72E-04	9.69E-01	5.39E+01
	3.56E-03	9.48E-01	2.30E+02	1.30E-04	9.75E-01	7.86E+01	1.17E-04	9.80E-01	4.04E+01
	3.59E-03	8.33E-01	2.26E+02	1.15E-04	8.99E-01	6.09E+01	1.42E-04	8.45E-01	2.76E+01
	3.72E-03	9.64E-01	2.28E+02	9.74E-05	9.39E-01	7.96E+01	8.95E-05	9.79E-01	3.35E+01
	3.70E-03	8.51E-01	2.23E+02	8.92E-05	9.54E-01	5.76E+01	1.18E-04	8.66E-01	2.35E+01
	3.85E-03	8.89E-01	2.18E+02	6.18E-05	9.71E-01	5.08E+01	8.62E-05	9.47E-01	2.29E+01
MgSO$_4$–MgCl$_2$–H$_2$O	2.97E-03	9.61E-01	2.45E+02	1.67E-04	8.57E-01	5.84E+01	2.31E-04	6.39E-01	5.27E+01
	3.46E-03	9.31E-01	2.36E+02	8.67E-05	9.37E-01	4.68E+01	9.40E-05	9.72E-01	3.57E+01
	3.53E-03	9.41E-01	2.32E+02	1.48E-04	9.71E-01	8.15E+01	1.15E-04	8.52E-01	4.00E+01
	3.79E-03	9.50E-01	2.26E+02	1.11E-04	9.60E-01	6.38E+01	8.91E-05	8.10E-01	3.56E+01
	3.14E-03	9.07E-01	2.43E+02	1.06E-04	7.15E-01	5.16E+01	1.60E-04	9.46E-01	4.86E+01
	2.98E-03	9.59E-01	2.35E+02	2.32E-04	8.23E-01	7.19E+01	3.07E-04	7.84E-01	5.90E+01
	3.22E-03	9.14E-01	2.44E+02	7.96E-05	9.02E-01	3.11E+01	1.15E-04	9.80E-01	2.92E+01
	3.31E-03	9.68E-01	2.44E+02	5.20E-05	9.74E-01	2.88E+01	6.67E-05	9.80E-01	3.32E+01
	3.05E-03	9.60E-01	2.37E+02	2.04E-04	9.17E-01	7.17E+01	2.71E-04	9.66E-01	5.75E+01

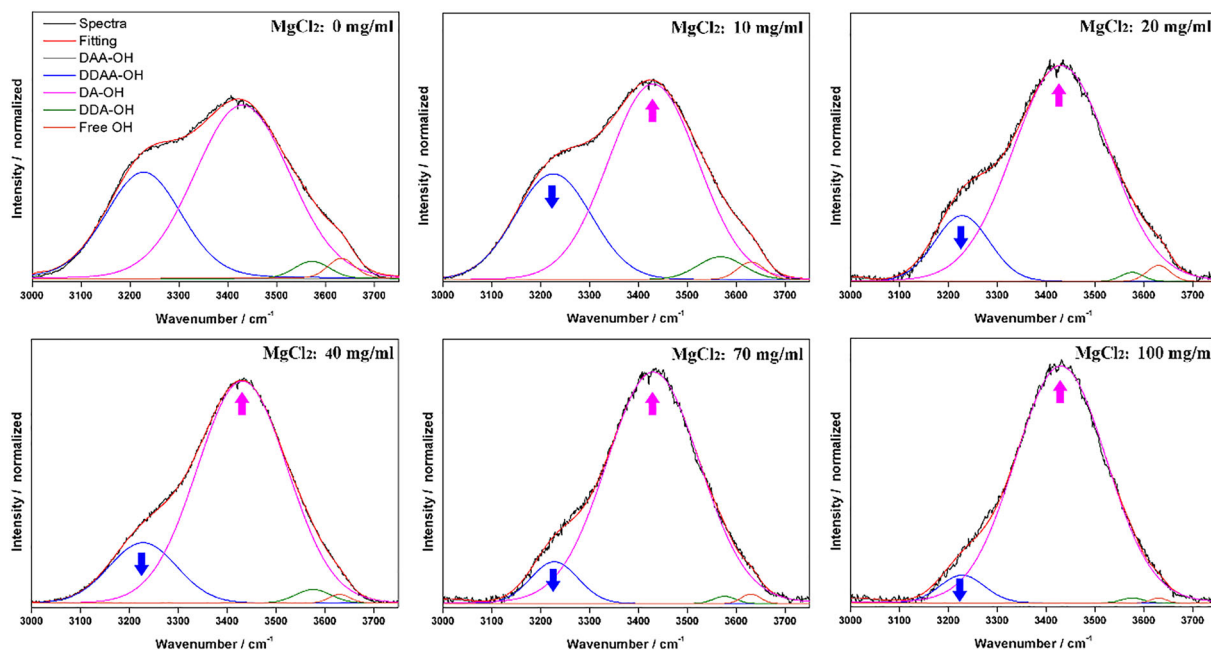**FIGURE 2** OH band fitting of representative MgCl–H_2O solution, presenting the original (black line) and band fitted (red) spectra, as well as the sub-bands representing DAA (gray), DDAA (blue), DA (pink), DDA (green), and free OH (orange) vibrational modes
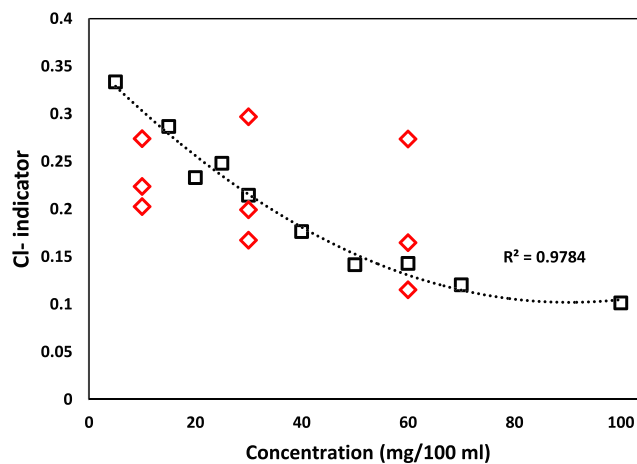

FIGURE 3 Calibration curve to semi-quantify the Cl^- content in water solutions. Black markers represent the 20 spectra-averaged values of mono-analyte $MgCl_2$ solutions, whereas red markers represent binary $MgSO_4$–$MgCl_2$ solutions.

The coefficient of correlation ($R^2 = 0.9784$) confirms that Raman spectroscopy can be used to semi-quantify the chloride content in water solutions, even though this monoatomic anion is Raman-inactive. However, similar to what is depicted in Figure 1, the semi-quantification model fails to correctly estimate the Cl^- content in case the solution contains additional anions (in this work sulfates). Focusing on sulfate and chloride mixtures (this being the predicted composition of the future scientific targets of the Europa lander), previous studies successfully determined the content of one of the salts, provided that the concentration of the second one is known. For instance, knowing the chloride content of geologic fluid inclusions, Qiu et al. (2020) were able to semi quantify their sulfate content by building a dedicated calibration curve based on a set of Cl^-–SO_4^{2-} solutions in which the concentration of chloride was fixed at 6.3 mol/kg (27 mass%).[46]

However, the perturbations created by the mixture of multiple salts on the OH profile of the water are so complex that univariate semi-quantitation models are not able to successfully determine the concentration of both chlorides and sulfates. To overcome the limitations of univariate calibration curves, ANNs have been employed to create semi-
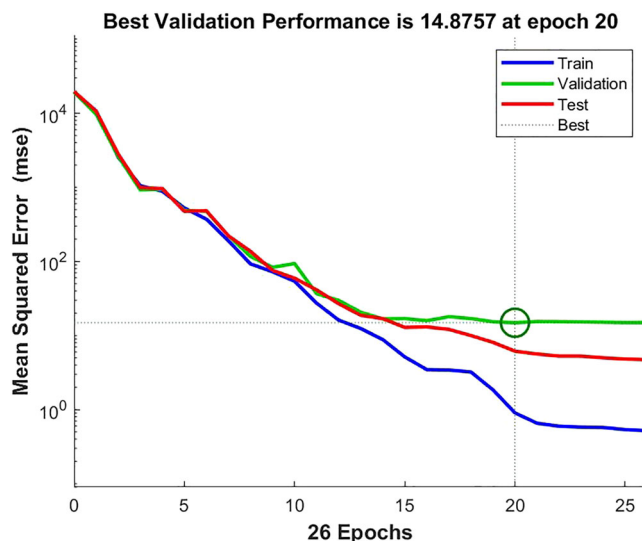
FIGURE 4   Best validation performance in artificial neural network
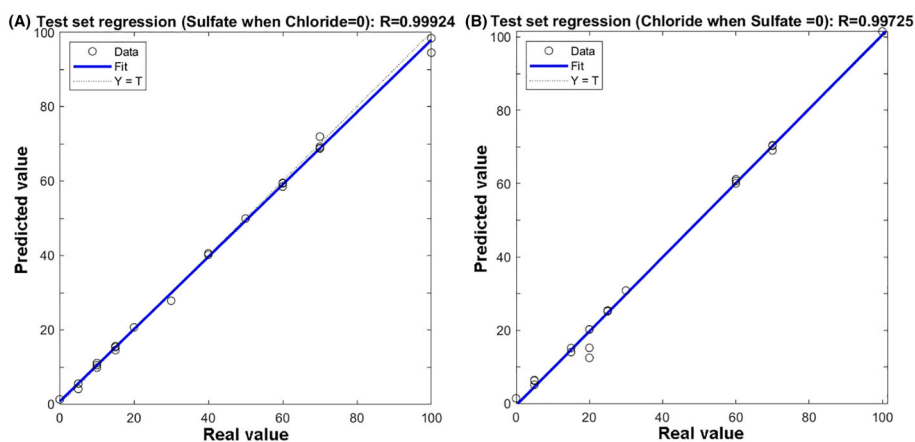

FIGURE 5   Correlation between actual and predicted values from the analysis of mono-ionic water solutions using ANN. Sulfate (A) and chloride (B) test set regressions.

quantitative models that consider all spectral parameters extrapolated by the band fitting process of Raman spectra. In this sense, the neural network input consists of a data matrix of 620 rows (corresponding to the 31 solutions listed in Table 1, multiplied by the 20 collected spectra per sample) and 16 columns (intensity, width and Gaussian/Lorentzian ratio of the five vibrational modes of the OH region, together with the intensity of the main peak of SO_4^{2-}). As explained in section 2.3, 70% of the input data were used for training, 15% for validation, and 15% for test.

The training of the ANN-based model followed an iterative process based on the use of a variable number of neurons in the hidden layer (from 10 to 50). The training was run five times for each network configuration. Then, the best-performing network was selected based on the resulting root mean square error. The optimization was carried out using a Levenberg–Marquardt algorithm for training. As detailed elsewhere,[51] the neuron parameters are recursively adjusted during training to fit the expected outputs, whereas validation and test sets are used to avoid overtraining the network. After training, the network was used with the whole data set to calculate the estimated concentration of both Cl^- and SO_4^{2-} in the solution. The coefficient of determination (R^2) value was considered for investigation of the prediction capability of the ANN, whereas the estimation capability was determined by comparing predicted and real values.[52] Figure 4 presents the Mean Squared Error (MSE) of ANN model for training, validation, and test steps. According to this figure, the least MSE in the validation step happens at epoch 20 which has the best validation performance equal to 14.8757.
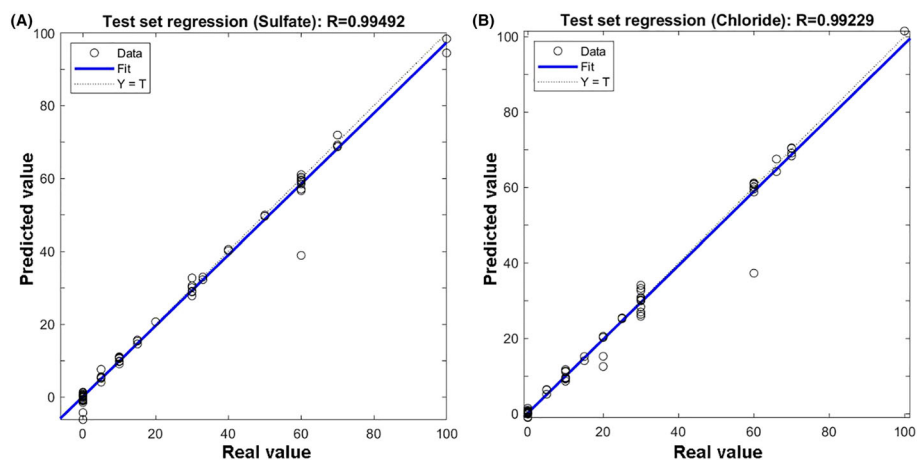
FIGURE 6 Correlation between actual and predicted values from the analysis of binary water solutions using ANN. Sulfate (A) and chloride (B) test set regressions.

Starting from the analysis of mono-anionic solutions (Table 1a and b), the R^2 obtained from the study of SO_4^{2-}–H_2O and Cl^-–H_2O solutions are 0.9992 and 0.9973, respectively (see Figure 5). Compared with the results provided by the calibration curves displayed in Figure 1 ($R^2 = 0.9978$) and Figure 3 ($R^2 = 0.9784$), the ANN model proved better prediction performance than the linear univariant models.

Afterwards, the same ANN was used to predict the saline content of both mono-analyte and binary solutions. Fitting result comparison showed significant predictions improvement of ANN compared with the calibration curves presented previously. As presented in Figure 6, the estimation of chloride and sulfate content in water solutions ensure a coefficient of determination of 0.9949 and 0.9923 respectively.

4 | CONCLUSION

In this work, the RLS-Sim has been used to predict the capability of the future Raman spectrometer onboard the Europa Lander to semi-quantify the saline content of water samples. Focusing on the use of calibration curves, the RLS-Sim was successfully used to determine the sulfate and chloride contents of mono-analyte solutions. Comparing the coefficients of correlation (0.9978 and 0.9784 for SO_4^{2-} and Cl^-, respectively) with those obtained in previous works, this research proves the lower analytical performances of Raman spectrometers for planetary missions (over state-of-the-art laboratory systems) can be partially compensated by increasing the number of spectra captured from each sample.

However, this research analytically confirmed that standard calibration curves are not suitable for the semi quantification of complex water solutions in which multiple salts are present. Indeed, the dissolved anions produce critical perturbations of the fundamental OH band of the water, which is typically used as the internal spectral parameter for normalization purposes. In this sense, Figure 3 clearly shows the intensity of DDAA and DA vibrational modes are strongly affected by the salinity of the solution (although further variations are observed). To overcome this issue, a second semi-quantification method based on ANNs has been tested. Through the automated band fitting of the OH region, the key spectral parameters describing the five main OH vibrational modes were used as inputs of the ANN. After training, validation and test, the coefficient of correlation obtained by ANN was above 0.999 for both mono-analyte and binary solutions. The capability of the ANN to successfully predict the concentration of both chloride and sulfate in binary solutions can be attributed to the fact that, by evaluating a wider set of spectral parameters, the non-linearity prediction ability of ANN allows (unlike calibration curves) to successfully resolve the complexity of the OH perturbation caused by the presence of multiple ions. As such, the combination of Raman analysis and ANN represents a valuable approach to successfully achieve the semi-quantification of saline solution on Europa.

To better understand the OH perturbation dynamics triggered by dissolved salts, the combination of Raman spectroscopy and ANN will be extended to the determination of additional saline solutions. In addition to that, knowing the vibrational profile of OH is also affected by temperature and pressure conditions, further studies will be performed at

environmental conditions representative of Europa. In this sense, the present work must be seen as the first step of a research line that is aimed at optimizing the potential scientific outcome of Raman spectrometers applied to the exploration of Europa and further icy planets.

ACKNOWLEDGEMENTS

ORCID

Jose Antonio Manrique https://orcid.org/0000-0002-2053-2819
Marco Veneranda https://orcid.org/0000-0002-7185-2791
Guillermo Lopez-Reyes https://orcid.org/0000-0003-1005-1760

REFERENCES

1. Farley KA, Williford KH, Stack KM, et al. Mars 2020 Mission overview. *Space Sci Rev*. 2020;216(8):142. doi:10.1007/s11214-020-00762-y
2. Wiens RC, Maurice S, Robinson SH, et al. The SuperCam instrument suite on the NASA Mars 2020 rover: body unit and combined system tests. *Space Sci Rev*. 2020;217:4.
3. Manrique JA, Lopez-Reyes G, Cousin A, et al. SuperCam calibration targets: design and development. *Space Sci Rev*. 2020;216:138.
4. Maurice S, Wiens RC, Bernardi P, et al. The SuperCam instrument suite on the Mars 2020 rover: science objectives and mast-unit description. *Space Sci Rev*. 2021;217(3):4747. doi:10.1007/s11214-021-00807-w
5. Hollis JR, Abbey W, Beegle LW, et al. A deep-ultraviolet Raman and fluorescence spectral library of 62 minerals for the SHERLOC instrument onboard Mars 2020. *Planet Space Sci*. 2021;209:105356. doi:10.1016/j.pss.2021.105356
6. Allwood AC, Wade LA, Foote MC, et al. PIXL: planetary instrument for X-ray Lithochemistry. *Space Sci Rev*. 2020;216(8):134. doi:10.1007/s11214-020-00767-7
7. Muirhead BK, Nicholas AK, Umland J, Sutherland O, Vijendran S. Mars sample return campaign concept status. *Acta Astronaut*. 2020;176:131-138. doi:10.1016/j.actaastro.2020.06.026
8. Vago JL, Westall F, Pasteur Instrument Teams, et al. Habitability on early Mars and the search for biosignatures with the ExoMars rover. *Astrobiology*. 2017;17(6-7):471-510. doi:10.1089/ast.2016.1533
9. Rull F, Maurice S, Hutchinson I, et al. The Raman laser spectrometer for the ExoMars rover Mission to Mars. *Astrobiology*. 2017;17(6-7):627-654. doi:10.1089/ast.2016.1567
10. Bibring JP, Hamm V, Pilorget C, Vago JL. The MicrOmega investigation onboard ExoMars. *Astrobiology*. 2017;17(6-7):621-626. doi:10.1089/ast.2016.1642
11. Goesmann F, Brinckerhoff WB, Raulin F, et al. The Mars organic molecule analyzer (MOMA) instrument: characterization of organic material in Martian sediments. *Astrobiology*. 2017;17(6-7):655-685. doi:10.1089/ast.2016.1551
12. Russell MJ, Murray AE, Hand KP. The possible emergence of life and differentiation of a shallow biosphere on irradiated icy worlds. *Astrobiology*. 2017;17(12):1265-1273. doi:10.1089/ast.2016.1600
13. Kimura J, Kitadai N. Polymerization of building blocks of life. *Astrobiology*. 2015;15(6):430-441. doi:10.1089/ast.2015.1306
14. Greenberg R, Geissler P. Invited review Europa's dynamic icy crust. *Meteorit Planet Sci*. 2002;37(12):1685-1710. doi:10.1111/j.1945-5100.2002.tb01158.x
15. National Research Council. *New Frontiers in the Solar System: An Integrated Exploration Strategy*. The National Academies Press; 2003.
16. National Research Council. *Vision and Voyages for Planetary Science in the Decade 2013-2022*. The National Academies Press; 2011.
17. Howell SM, Pappalardo RT. NASA's Europa clipper — a mission to a potentially habitable ocean world. *Nat Commun*. 2020;9–12(1): doi:10.1038/s41467-020-15160-9
18. Hand KP, Phillips CB, Murray A, et al. Science goals and Mission architecture of the Europa Lander Mission concept. *Planet Sci J*. 2022;22:1-31.
19. Sharma SK, Porter JN, Misra AK, Acosta-Maeda TE, Angel SM, McKay CP. Standoff Raman spectroscopy for future Europa Lander missions. *J Raman Spectrosc*. 2020;51(9):1782-1793. doi:10.1002/jrs.5814
20. Mellerowicz B, Zacny K, Eshelman E, et al. Development of a Deep Drill System with Integrated UV/Raman Spectrometer for Mars and Europa. In *2018 AIAA SPACE and Astronautics Forum and Exposition*; 2018:124. doi:10.2514/6.2018-5290.
21. Lambert J, Wang A. Overview of the Compact Integrated Raman Spectrometer (CIRS) for an Europa Lander Mission James. In *2019 Astrobioligy Science Conference*; 2019: 415.
22. Gershman R, Nilsen E, Oberto R. Europa Lander. *Acta Astronaut*. 2003;52(2-6):253-258. doi:10.1016/S0094-5765(02)00164-9
23. Gleeson DF, Anderson MS, Grasby SE, Mielke RE, Pappalardo RT. Biosignature detection at an Arctic analog to Europa. *Astrobiology*. 2012;12(2):135-150. doi:10.1089/ast.2010.0579

24. Gleeson DF, Pappalardo RT, Grasby SE, et al. Remote sensing of environment characterization of a sulfur-rich Arctic spring site and fi eld analog to Europa using hyperspectral data. *Remote Sens Environ*. 2010;114(6):1297-1311. doi:10.1016/j.rse.2010.01.011

25. Lorenz RD, Gleeson D, Prieto-Ballesteros O, Gomez F, Hand K, Bulat S. Analog environments for a Europa lander mission. *Adv Sp Res*. 2011;48(4):689-696. doi:10.1016/j.asr.2010.05.006

26. Klenner F, Postberg F, Hillier J, et al. Analog experiments for the identification of trace biosignatures in ice grains from. *Astrobiology*. 2020;20(2):1-11. doi:10.1089/ast.2019.2065

27. Mason DP, Madden MEE. Raman spectroscopy of high salinity brines and ices. *Icarus*. 2022;372:114759. doi:10.1016/j.icarus.2021.114759

28. Thomas EC, Hodyss R, Vu TH, Johnson PV, Choukroun M. Composition and evolution of frozen chloride brines under the surface conditions of Europa. *Earth Sp Chem*. 2017;1(1):14-23. doi:10.1021/acsearthspacechem.6b00003

29. Muñoz-Iglesias V, Bonales LJ, Prieto O, pH and Salinity Evolution of Europa's Brines: Raman Spectroscopy Study of Fractional. *Astrobiology*. 2013;13:693-702. doi:10.1089/ast.2012.0900

30. Mckinnon WB, Zolensky ME. Sulfate Content of Europa's Ocean and Shell: Evolutionary Considerations and Some Geological and Astrobiological Implications. *Astrobiology*. 2003;3(4):879-897. doi:10.1089/153110703322736150

31. Trumbo SK, Brown ME, Hand KP. Sodium chloride on the surface of Europa. *Sci Adv*. 2019;5:eaw7123.

32. Marion G, Fritsen C, Eicken H. The search for life on Europa: limiting environmental factors, potential habitats, and Earth analogues. *Astrobiology*. 2003;3(4):785-811. doi:10.1089/153110703322736105

33. Chela-Flores J, Kumar N. Returning to Europa : can traces of surficial life be detected? *Int J Astrobiol*. 2008;7(3-4):263-269. doi:10.1017/S1473550408004242

34. Zolotov MY, Shock EL. Energy for biologic sulfate reduction in a hydrothermally formed ocean on Europa. *J Geophys Res*. 2003;108(E4):5022. doi:10.1029/2002JE001966

35. Mabrouk KB, Kauffmann TH, Fontana MD. Raman study of cation effect on sulfate vibration modes in solid state and in aqueous solutions. *J Raman Spectrosc*. 2013;44(11):1603-1608. doi:10.1002/jrs.4374

36. Kauffmann TH, Fontana MD. Sensors and actuators B : chemical inorganic salts diluted in water probed by Raman spectrometry : data processing and performance evaluation. *Sens Actuators B*. 2015;209:154-161. doi:10.1016/j.snb.2014.11.108

37. Boiron MA, Dubessy J, Rull F. Determination of Chlorinity in aqueous fluids using Raman spectroscopy of the stretching band of water at room temperature : application to fluid inclusions. *Appl Spectrosc*. 2002;56(1):99-106. doi:10.1366/0003702021954278

38. Sun Q, Zhao L, Li N, Liu J. Raman spectroscopic study for the determination of $cl-$ concentration (molarity scale) in aqueous solutions : application to fluid inclusions. *Chem Geol*. 2010;272(1-4):55-61. doi:10.1016/j.chemgeo.2010.02.004

39. Gajaraj S, Fan C, Lin M. Quantitative detection of nitrate in water and wastewater by surface-enhanced Raman spectroscopy. *Environ Monit Assess*. 2013;185(7):5673-5681. doi:10.1007/s10661-012-2975-4

40. Liu J, Osadchy M, Ashton L, Foster M, Solomon CJ, Gibson SJ. Deep convolutional neural networks for Raman spectrum recognition : a unified solution. *Analyst*. 2017;142(21):4067-4074. doi:10.1039/C7AN01371J

41. Lopez-Reyes G, Veneranda M, Manrique JA, et al. RLS Sim: A heavy-duty Raman tool for ground testing on ExoMars. *J Raman Spectrosc*. 2022;53(3):382-395.

42. Lopez-Reyes G, Rull Pérez F. A method for the automated Raman spectra acquisition. *J Raman Spectrosc*. 2017;48(11):1654-1664. doi:10.1002/jrs.5185

43. Veneranda M, Saiz J, Lopez-Reyes G, et al. PTAL, ADAMM and SpectPro : novel tools to support ExoMars and Mars 2020 science operations. In *Europlanet Science Congress*; 2020.

44. Saiz J, Lopez-Reyes G, Veneranda M, *et al*. Automated sample identification with SpectPro and PTAL database for the analysis of spectra from planetary missions. In *EGU General Assembly 2019*. 2019; 21:17904.

45. Zhu D, Zhu Z, Pan J, Ding J, Ni P. Raman Micro-spectroscopic study of sulfate ion in the system Na_2SO_4-H_2O. *Acta Geol Sin*. 2015;89(3):887-893. doi:10.1111/1755-6724.12486

46. Qiu Y, Yang Y, Wang X, et al. In situ Raman spectroscopic quantification of aqueous sulfate : experimental calibration and application to natural fluid inclusions. *Chem Geol*. 2020;533:119447. doi:10.1016/j.chemgeo.2019.119447

47. Sun Q. Vibrational spectroscopy the Raman OH stretching bands of liquid water. *Vib Spectrosc*. 2009;51(2):213-217. doi:10.1016/j.vibspec.2009.05.002

48. Pezzotti G, Puppulin L, la Rosa A, et al. Effect of pH and monovalent cations on the Raman spectrum of water: basics revisited and application to measure concentration gradients at water/solid interface in Si 3 N 4 biomaterial. *Chem Phys*. 2015;463:120-136. doi:10.1016/j.chemphys.2015.10.010

49. Cappa CD, Smith JD, Messer BM, Cohen RC, Saykally RJ. Effects of cations on the hydrogen bond network of liquid water : new results from X-ray absorption spectroscopy of liquid microjets. *J Phys Chem B*. 2006;110(11):5301-5309. doi:10.1021/jp054699c

50. Yuan X, Mayanovic RA. An empirical study on Raman peak fitting and its application to Raman quantitative research. *Appl Spectrosc*. 2017;71(10):2325-2338. doi:10.1177/0003702817721527

51. Manrique-Martinez JA, Lopez-Reyes G, Alvarez-Perez A, et al. Evaluation of multivariate analyses and data fusion between Raman and laser-induced breakdown spectroscopy in binary mixtures and its potential for solar system exploration. *J Raman Spectrosc*. 2020;1–16 (9):1702-1717. doi:10.1002/jrs.5819

52. Selin Uysal R, Hakki I, Efe H, Tamer U. Determination of butter adulteration with margarine using Raman spectroscopy. *Food Chem*. 2013;141(4):4397-4403. doi:10.1016/j.foodchem.2013.06.061